Boundary-Layer Meteorol (2012) 144:157–177
DOI 10.1007/s10546-012-9716-7

ARTICLE

On Monin–Obukhov Scaling in and Above the Atmospheric Surface Layer: The Complexities of Elevated Scintillometer Measurements

Miranda Braam · Fred C. Bosveld · Arnold F. Moene

Received: 13 May 2011 / Accepted: 6 March 2012 / Published online: 31 March 2012

Abstract In scintillometry Monin–Obukhov similarity theory (MOST) is used to calculate the surface sensible heat flux from the structure parameter of temperature (C_{T^2}). In order to prevent saturation a scintillometer can be installed at an elevated level. However, in that case the observation level might be located outside the atmospheric surface layer (ASL) and thus the validity of MOST questioned. Therefore, we examine two concepts to determine the turbulent surface sensible heat flux from the structure parameter at elevated levels with data obtained at 60-m height on the Cabauw tower (the Netherlands). In the first concept (MOSTs) C_{T^2} is still scaled with the surface flux, whereas in the second (MOSTl) C_{T^2} is scaled with the local sensible heat flux. The C_{T^2} obtained from both concepts is compared with direct observations of C_{T^2} using a sonic anemometer/thermometer. In the afternoon (when the measurement height is located within the ASL) both concepts give results that are comparable to the directly observed values of C_{T^2}. In the morning (data outside the ASL), our data do not unequivocally support either of the two concepts. First, the peak in C_{T^2} that occurs when the measurement height is located in the entrainment zone disqualifies the use of MOST. Second, during the morning transition, local scaling shows the correct pattern (zero flux and a minimum in C_{T^2}) but underestimates C_{T^2} by a factor of ten. Third, from the best linear fit a we found that the slope of MOSTl gave better results, whereas the offset

M. Braam (✉) · A. F. Moene
Meteorology and Air Quality Group, Wageningen University,
PO Box 47, 6700 AA Wageningen, The Netherlands
e-mail: miranda.braam@wur.nl

A. F. Moene
e-mail: arnold.moene@wur.nl

M. Braam
Deutscher Wetterdienst, Meteorologisches Observatorium Lindenberg,
Am Observatorium 12, 15848 OT Tauche Lindenberg, Germany

F. C. Bosveld
Department of Regional Climate, Royal Netherlands Meteorological Institute,
Wilhelminaweg 10, 3732 GK De Bilt, The Netherlands
e-mail: fred.bosveld@knmi.nl

is closer to zero for MOSTs. Further, the correlation between the direct observations and MOST-scaled results is low and similar for the two concepts. In the end, we conclude that MOST is not applicable for the morning hours when the observation level is above the ASL.

Keywords Elevated levels · Monin–Obukhov similarity theory · Morning transition · Scintillometry · Structure parameter of temperature

1 Introduction

The area-averaged surface flux of sensible heat is of interest for many meteorological and hydrological studies, e.g. to evaluate mesoscale numerical models or satellite-based retrieval algorithms. Over homogeneous terrain, the eddy-covariance method or other local point measurement techniques can be used to determine this flux (Lee et al. 2004; Foken 2008). Over heterogeneous terrain, however, point measurements are not suitable. During recent years, the use of scintillometers has proven to be a reliable method for measuring the spatially-averaged flux over heterogeneous surfaces under daytime conditions (e.g. Meijninger et al. 2002; Beyrich et al. 2005; Kohsiek et al. 2006). To obtain the sensible heat flux from the scintillometer signal several steps are involved. From the scintillometer data the structure parameter of the refractive index of air is determined, which is used to calculate the structure parameter of temperature (C_{T^2}). Then, the surface sensible heat flux is derived by applying Monin–Obukhov similarity theory (MOST) (Wyngaard 1973; Meijninger 2003; Moene et al. 2004), which is valid for the atmospheric surface layer (ASL), where fluxes are assumed to vary little with height.

One limitation of the scintillometer is that it has an upper limit on scintillations that can be measured, due to the saturation of the scintillometer signal (Kohsiek et al. 2002, 2006). One way to prevent saturation is to install a scintillometer at an elevated level, since the magnitude of the structure parameter of temperature decreases with height. However, a consequence of a greater height is that the observations are not always located in the ASL and the application of MOST is in principle not justified. This situation particularly occurs in the morning when the boundary layer is relatively shallow.

In order to obtain the surface sensible heat flux from the structure parameter of temperature at elevated levels under unstable conditions, two different theoretical concepts are proposed. In the first concept, we assume that MOST still applies at levels just above the ASL and that C_{T^2} still scales with the surface flux. In the second concept, the structure parameter of temperature at elevated levels has to be scaled with the local sensible heat flux, rather than with the surface flux. To obtain the surface heat flux a correction for the flux divergence in the column below the level of observation has to be applied.

Whereas the scintillometer is the motivation of our study, we chose to evaluate the two proposed concepts with data from a sonic anemometer/thermometer (sonic) installed on the Cabauw tower, the Netherlands, about 60 m above the surface. The footprint of the path-averaged C_{T^2} obtained by the scintillometer differs from the footprint of the sensible heat fluxes (point measurements), which are calculated from sonic data. Consequently, the main question is how the surface sensible heat flux should be determined from the structure parameter of temperature determined at 60 m under unstable conditions, particularly during the morning period when the level of 60 m is situated above the ASL. Since several MOST relationships are proposed in the literature (see Moene et al. 2004), we perform an analysis of the relationships of Andreas (1988), Hill et al. (1992) and de Bruin et al. (1993) (hereafter referred to

A88, H92 and DB93, respectively) before comparing the two concepts, to investigate which similarity relationship is most suitable for our dataset.

The paper is structured as follows: in Sect. 2 the theory behind MOST and the two proposed concepts are described. Information about the experimental set-up, dataset and the applied corrections can be found in Sect. 3. Section 4 provides a description of the boundary-layer structure, a similarity study of the MOST relationships with the data observed in the ASL is presented, and the two proposed concepts are compared. In the final section the conclusions are given.

2 Theory

Monin–Obukhov similarity theory applies to the ASL (with depth z_{ASL}) under stationary and horizontally homogeneous surface conditions (e.g. Businger et al. 1971). In the ASL, turbulence is controlled by surface processes, whereas processes in the rest of the atmospheric boundary layer (with depth z_{i}), such as entrainment, play a less important role. For this reason, the only height in the dimensional analysis that is taken into account is the observation height (z). This holds if $z \ll z_{\mathrm{i}}$, which is operationalized as $z < 0.1 z_{\mathrm{i}}$. If we assume a linear sensible heat-flux profile and no entrainment at the top of the boundary layer then surface-layer fluxes do not differ by more than 10 % from the surface flux ($\overline{w'T'}_{\mathrm{s}}$) within the surface layer, as is illustrated in Fig. 1 by the solid line. Therefore, the surface layer is often referred to as the constant-flux layer. However, in the case of dry air entrainment, the variation in the heat flux is more than 10 % over the depth of the ASL ($0.1 z_{\mathrm{i}}$) (Fig. 1). The dashed line represents a case for the free convection situation with an entrainment flux ($\overline{w'T'}_{\mathrm{e}}$) that amounts to -0.2 ($\overline{w'T'}_{\mathrm{s}}$) (Tennekes 1973). In that case the fluxes across the surface layer do not vary that much: 12 %. During the morning period however, when the entrainment flux is large (dash-dotted line) the fluxes within the ASL can differ much more. From our dataset we find an entrainment ratio of -1.2, 2 h after sunrise. This gives a flux variation of 22 % across the ASL. Consequently, the application of MOST at elevated levels is questionable in the morning period for two reasons: (a) the relative height z/z_{i} of a certain observation level

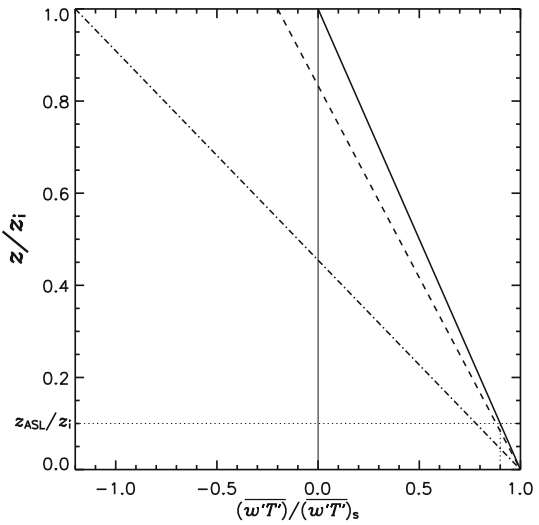

Fig. 1 Three sketches of the linear turbulent sensible heat-flux profile in the boundary layer. *Solid line* without an entrainment flux ($\overline{w'T'}_{\mathrm{e}} = 0$). *Dashed line* free-convection situation ($\overline{w'T'}_{\mathrm{e}} = -0.2\overline{w'T'}_{\mathrm{s}}$). *Dash-dotted line* early morning situation ($\overline{w'T'}_{\mathrm{e}} = -1.2\overline{w'T'}_{\mathrm{s}}$)

can easily be larger than 0.1 if the boundary layer is shallow, and (b) the flux divergence in the surface layer can be larger than 10 % when (the absolute value of) the entrainment ratio is large. Kohsiek (1988) used mixed-layer scaling to scale structure parameters at levels up to 200 m under convective conditions. This approach may be also questionable in the early morning when the boundary layer is not yet well-mixed.

MOST is based on the observation that the statistics of turbulence in the surface layer are fully determined by four parameters: the surface flux of the scalar under consideration, the friction velocity u_*, the buoyancy flux $g/(T\overline{w'T_v'})$ and the height above the surface z (Wyngaard 1973; Stull 1988; Meijninger 2003; Moene et al. 2004). Applying this to the structure parameter of temperature we obtain:

$$\frac{C_{T^2} z^{2/3}}{T_*^2} = f\left(\frac{z}{L}\right) \tag{1}$$

with the Obukhov length $L = T{u_*}^2/(\kappa g T_{v*})$, the temperature scale $T_* = -H/(\rho c_\mathrm{p} u_*)$ and the friction velocity $u_* = \sqrt{\tau_0/\rho}$, in which T is the temperature, T_v is the virtual temperature, $\kappa = 0.4$ is the von Karman constant, $g = 9.81\,\mathrm{m\,s^{-1}}$ is the gravity acceleration, H is the surface sensible heat flux, ρ is the density, c_p is the specific heat at constant pressure and τ_0 is the surface shear stress. Several expressions for $f\ (z/L)$ exist in the literature for stable and unstable conditions (for an overview see Moene et al. 2004). Since we focus our research on unstable conditions only, the formulations of H92, A88 and DB93 are evaluated (Table 1). The relationships all have the form:

$$f\left(\frac{z}{L}\right) = c_1\left(1 - c_2\frac{z}{L}\right)^{-2/3} \tag{2}$$

in which the coefficients (c_1 and c_2) have been empirically determined with near-surface data by varying L. The coefficient c_1 is the asymptotic value of $f\ (z/L)$ for the neutral limit. On the other hand, $1/c_2$ is a measure of stability (z/L) at which the neutral limit transits into the free convection limit. The exponent $-2/3$ ensures the correct behaviour in the free convection limit. The fourth and fifth columns in Table 1 display the observation level and the stability range for the datasets on which the relationships are based. For near-neutral conditions the H92 relationship gives the highest values, due to the high value of c_1. The similarity relationships of DB93 and A88 have the same value of c_1. However, since c_2 is much higher for DB93, the transition point from neutral to unstable conditions occurs at a lower stability. As a result, the similarity relationship of DB93 shows the lowest values. Under very unstable conditions the three show quite similar results. In the free convection

Table 1 Expressions for the similarity relationships ($f\ (z/L) = c_1\ (1 - c_2 z/L)^{-2/3}$) under unstable conditions. Note that the similarity relationship of A88 is a modification of Wyngaard (1973) with $\kappa = 0.4$

c_1	c_2	d	Observation level (m)	Stability range	Reference
4.9	6.1	1.46	5.66, 11.3 and 22.6	Scattered cloud$-z/L < 1.1$	Andreas (1988)
				six points: $1.1 < -z/L < 2.5$	
8.1	15	1.33	3.95	50 % of data: $0.1 < -z/L < 0.5$	Hill et al. (1992)
4.9	9	1.13	11.3	Scattered cloud: $-z/L < 3$	de Bruin et al. (1993)
				six points: $3 < -z/L < 100$	

limit Eq. 2 reduces to $f = d\,(-z/L)^{-2/3}$ in which $d = c_1 c_2^{-2/3}$; d is also given in Table 1 showing that A88 gives largest and DB93 gives lowest values in the free convective range.

As discussed above, MOST might not be expected to be valid at the measurement height during the morning period due to the shallow surface layer and the large entrainment flux. In order to obtain the surface sensible heat flux from the structure parameter of temperature at elevated levels, two different concepts are proposed.

In the first concept (MOSTs, s for surface), the structure parameter of temperature at 60 m is scaled with the surface flux. Although the surface flux may not affect the turbulence outside the ASL directly, it does so indirectly. The surface heat flux is the cause of the temperature contrast over the depth of the atmospheric boundary layer, and as such is the primary source of turbulent temperature fluctuations. Therefore the structure parameter, which is a measure of temperature fluctuations, will scale on the surface flux. Consequently, we hypothesize that MOST can be applied at higher levels as well. In the second concept (MOSTl, l for local level), the structure parameter is scaled with the local-level fluxes. The assumption is that there is a local relation between vertical heat transport and the smaller scale temperature fluctuations in the turbulent cascade towards the dissipation range. This use of MOST is comparable with the local scaling hypothesis that is often used in the stable boundary layer (Nieuwstadt 1984). In order to obtain the surface flux, a correction for the flux divergence between the surface and the observational level needs to be applied when using this concept.

3 Research Strategy and Methods

The data have been collected at the Cabauw tower (52°58.22′N 4°55.57′ E), which is located in the western part of the Netherlands. The area around the tower is open pasture terrain for 400 m; for a detailed description of the site area see van Ulden and Wieringa (1995). At first sight the surroundings of Cabauw have quite homogeneous surface characteristics, though on closer inspection a distinction has to be made between the regional characteristics and those close to the tower. First, the near-tower aerodynamic roughness length ($z_{0\mathrm{m}}$) is smaller than the regional value (grassland, $z_{0\mathrm{m}} \approx 0.03$ m and scattered rows of trees, $z_{0\mathrm{m}} \approx 0.15$ m, respectively). For a given geostrophic wind, the near-tower friction velocity will be different from the regional value. Second, we find a distinction between the near-tower and regional Bowen ratios (see Sect. 4.1). Since we investigate data from elevated levels that have a larger footprint area than surface observations, the regional surface characteristics are relevant for this study. Notice that, in this manuscript, the adjective near-tower (in contrast to regional) refers to the local horizontal area that influences the sonic measurements. This is done, because the adjective local-level (in contrast to surface) is already used to specify the local vertical measurement level used for scaling.

The analyzed period covers 4 May 2008 to 11 May 2008, a period chosen because it consists of cloud-free days, and the synoptic weather conditions show only little variation. Due to this small variation we are able to use a composite of the eight days for part of the analyses using 30-min averaged data.

This section starts with a description of the main steps in the analysis, which is supported by Fig. 2. Subsequently the methods of calculating fluxes and C_{T^2} from the sonic anemometer/thermometer (sonic) data (Sect. 3.2) and the determination of C_{T^2} from the scintillometer data are outlined (Sect. 3.3).

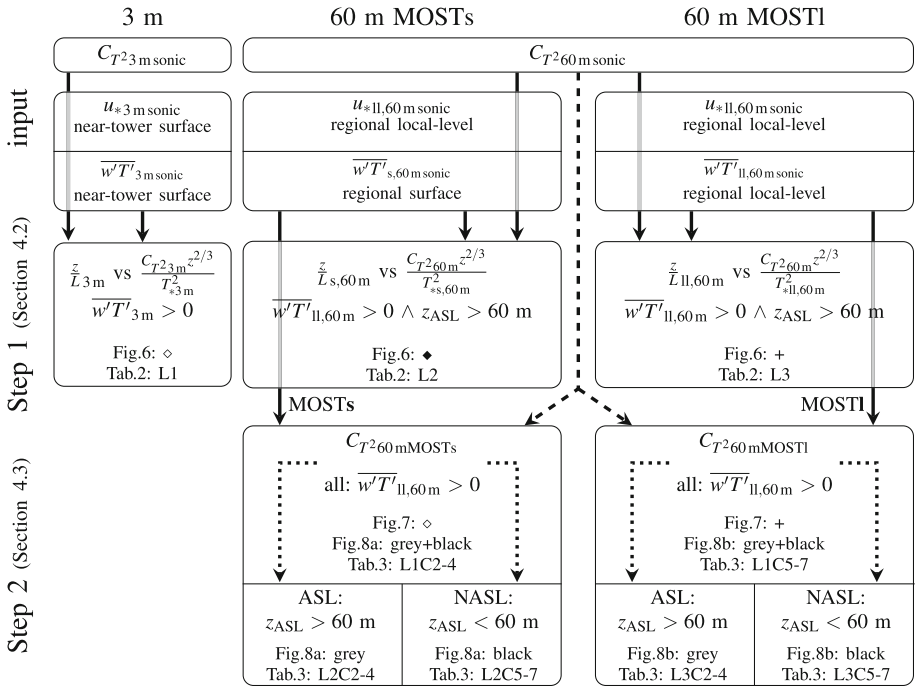

Fig. 2 Sketch of the research strategy. The first two rows represent the input data (the first the directly measured C_{T^2} and the second the combinations of friction velocity and turbulent sensible heat flux used in MOST). The second two rows show the output (first line), with which condition the data are filtered (second line) and in which Figure and Table the analysis is shown (last lines). *Solid arrows* mean 'is input of', the *dashed arrows* mean 'will be used to validate' and the dotted ones 'will be split into'. The abbreviation 'ASL' stands for atmospheric surface-layer data, 'NASL' for non-atmospheric surface-layer data, 'L' for line and 'C' for column

3.1 Research Strategy

This research can be split into two steps. In the first step we evaluate which of the proposed similarity relationships is valid for our dataset, while the second step evaluates the validity of the MOSTs and MOSTl concepts.

In both steps an independent measure of the structure parameter of temperature is needed (row 1, Fig. 2). In step 1 we need the independent C_{T^2} as input to compare the two dimensionless groups (z/L and $C_{T^2}z^{2/3}/T_*^2$) in MOST. In step 2 the independent C_{T^2} are used to validate the 60-m structure parameter of temperature calculated with the two different MOST concepts ($C_{T^2\mathrm{60mMOSTs}}$ and $C_{T^2\mathrm{60mMOSTl}}$). Ideally, we would use the scintillometer to determine the independent structure parameter, because the scintillometer measurements at elevated levels are the motivation behind our study. However, the MOST-scaling variables (row 2, Fig. 2) that are used in the validation cannot be obtained from the scintillometer but are available from the sonic measurements. So, then the footprints of the MOST-scaling variables (sonic: point measurements) will differ from that of the independent structure parameter (scintillometer: path measurements). Furthermore, the scintillometer does not measure C_{T^2} directly, but it is obtained from C_{n^2}. Therefore, we decided to analyze the directly observed C_{T^2} from the sonic instead of C_{T^2} derived from the scintillometer. Another advantage of

using the sonic is that data are also available at 3, 100 and 180 m. In other words, in this research the concepts are solely analyzed with sonic data (see Sect. 3.3 for details about the determination of C_{T^2} from the sonic), whereas the scintillometer is our motivation. Therefore, scintillometer output is only used to compare the path-averaged C_{T^2} with the point measured C_{T^2}, in order to ensure that our conclusions are relevant for scintillometer data as well.

Furthermore, both steps also need MOST scaling variables as input data (row 2, Fig. 2). Strictly speaking, the temperature scale and the friction velocity are calculated from the surface fluxes (see Sect. 2), but in practice H and τ_0 cannot be measured. Instead, the fluxes are derived from the turbulence fluxes measured with the sonic. For the scaling related to the 3-m data it is assumed that there is no vertical flux divergence so that the observed turbulence fluxes are equal to the near-tower surface fluxes (column 1 of row 2, Fig. 2). As said before a difference was found between the near-tower and the regional fluxes around Cabauw, therefore in the scaling related to the 60 m we use the regional fluxes. For the local-level scaling (MOSTl) this means that we are using the regional local-level friction velocity and the regional local-level turbulent heat flux. For the surface scaling (MOSTs), it is assumed that there is only flux divergence for the sensible heat flux. Hence, the regional surface sensible heat flux is derived from the observed flux at 60 m with a correction for the flux divergence. This correction is based on the time rate of change of the temperature as observed along the mast, where advection is neglected. Furthermore, in MOSTs we used $u_{*60\,\mathrm{m}}$ for the momentum flux. Consequently, the difference between MOSTl and MOSTs corresponds to the use of the regional local-level heat flux and the regional surface heat flux, respectively (column 2 and 3 of row 2, Fig. 2).

In order to evaluate which of the proposed similarity relationships (see Table 1) is valid for our dataset, we determine the similarity relationships for the 3-m data and the 60-m data (step 1, Fig. 2). In this analysis we focus on ASL data only, where MOST can be expected to be valid. As indicated in the previous section, the surface-layer depth is defined as 10 % of the boundary-layer depth. The boundary-layer depth is determined from a wind profiler (LAP 3000) following Beyrich and Görsdorf (1995) and Klein and Holtslag (1997). At 3 m (located in the ASL the entire time) all data under unstable conditions are selected ($\overline{w'T'}_{3\mathrm{m}} > 0$). For the 60-m level we consider only the unstable data where 60 m is located within the surface layer ($\overline{w'T'}_{\mathrm{ll,60m}} > 0 \wedge z_{\mathrm{ASL}} > 60\,\mathrm{m}$). Both MOSTs and MOSTl are used; due to the small variation of the flux with height within the surface layer MOSTs and MOSTl should show similar results.

The second step (Fig. 2) is to determine the validity of the MOSTs and MOSTl concepts at 60 m. We calculate the 60-m structure parameter of temperature with the two different MOST concepts ($C_{T^2\mathrm{60mMOSTs}}$ and $C_{T^2\mathrm{60mMOSTl}}$), and compare them with the directly observed values from the sonic ($C_{T^2\mathrm{60m\,sonic}}$). Note that the label sonic refers to the directly measured C_{T^2} without scaling, in contrast to the labels MOSTs and MOSTl that refer to C_{T^2} derived from sonic data by applying the scaling relation. The reason to use MOST in the reverse way (to obtain C_{T^2} from observed fluxes) is that we are interested in the different processes that act on the structure parameter of temperature rather than the flux itself. In our analysis all the data under unstable conditions are considered ($\overline{w'T'}_{\mathrm{ll,60m}} > 0$). In addition, the unstable data are split into two other groups. The first group contains data where 60 m is located in the ASL ($z_{\mathrm{ASL}} > 60\,\mathrm{m}$), whereas the second group consists of data obtained above the surface layer (during the early morning period, 'NASL', which represents non-atmospheric surface layer, $z_{\mathrm{ASL}} < 60\,\mathrm{m}$).

3.2 The Sonic Anemometer/Thermometer

The sonic anemometer/thermometer (Gill Solent R3, sample frequency: 10 Hz) is used, (a) to obtain the directly measured structure function of temperature ($C_{T^2\text{sonic}}$), and (b) to determine the turbulent fluxes that are used to calculate the MOST scaling parameters. The sonic path has a length of 0.15 m. Sonics are installed at 3, 60, 100 and 180 m height, with the sonic at 3 m positioned on a small mast approximately 200 m north of the main tower. The others are placed on the south-east booms of the tower. With easterly winds, as in the case for the period analyzed here, no significant flow obstruction occurs.

3.2.1 The Structure Parameter of Temperature

The structure parameter of temperature within the inertial subrange can be defined by (Stull 1988; Bosveld 1999; Moene et al. 2004):

$$C_{T^2} = \frac{D_{TT_x}(r)}{r^{\frac{2}{3}}} = \frac{\overline{[T(x+r) - T(x)]^2}}{r^{\frac{2}{3}}} \tag{3}$$

in which D_{TT_x} is the spatial (x) structure function, r is the spatial separation, $T(x)$ and $T(x+r)$ are the temperatures at location x and $x+r$. However from point observations (e.g. sonic data), only the temporal structure function of temperature (D_{TT_t}) can be derived:

$$D_{TT_t}(\tau) = \overline{[T(t+\tau) - T(t)]^2} \tag{4}$$

in which the subscript t indicates that it is the temporal structure function, $T(t)$ and $T(t+\tau)$ are temperatures at times t and $t+\tau$, and τ is the temporal separation. Lumley (1965) and Wyngaard and Clifford (1977) derive the conversion from the wavenumber to the frequency domain. Here we are concerned with the conversion from the time to space domain and follow Bosveld (1999). The conversion is performed by (a) assuming stationary and horizontally homogeneous conditions, (b) applying Taylor hypothesis, and (c) assuming that the turbulent variation of the wind vector has a three-dimensional Gaussian distribution:

$$D_{TT_x}(r) = \frac{D_{TT_t}(r/\overline{U})}{1 - \frac{1}{9}\frac{\sigma_u^2}{\overline{U}^2} + \frac{1}{3}\frac{\sigma_v^2}{\overline{U}^2} + \frac{1}{3}\frac{\sigma_w^2}{\overline{U}^2}} \tag{5}$$

in which, σ_x^2 is the variance of x, where x can be the wind component in the u, v and w direction respectively and $\overline{U}$ is the averaged length of the horizontal wind vector $\left(\sqrt{\overline{u(t)}^2 + \overline{v(t)}^2}\right)$. The variance in the three directions and the wind speed itself are determined with the sonic anemometer/thermometer. In this study we use fixed time lags; consequently, the spatial separation ($r = \tau\overline{U}$) varies in time. After investigating the width of the inertial subrange by spectral analysis (Braam 2008), we chose a time lag of 0.2 s for the sonic at 3 m and of 1.8 s for the other levels.

The temperature data from the sonic anemometer/thermometer are determined from the speed of sound. In the conversion from the so-called sonic temperature to the air temperature, the former is corrected for wind speed and humidity (Schotanus et al. 1983; Liu et al. 2001). The wind-speed correction is already done internally in the instrument (Gill Instruments Ltd. 2002). Essential variables in the humidity correction are specific humidity and mean temperature. Since the sonic cannot measure the absolute value of the temperature very accurately, we used the mean air temperature ($\overline{T}$) measured with KNMI Pt500-elements at 200, 140, 80,

40, 20, 10 and 1.5 m in the humidity correction. To determine the mean temperature at the height of the sonics, a linear interpolation between the two nearest levels is done. Based on the correction for temperature fluctuations (first part of Eq. 6 of Schotanus et al. (1983) and Eq. 10 of Liu et al. (2001)), the temporal structure function corrected for humidity becomes:

$$\overline{[T_{\mathrm{cor}}(t+\tau)-T_{\mathrm{cor}}(t)]^2}=\overline{\left[T_{\mathrm{son}}(t+\tau)-T_{\mathrm{son}}(t)+0.51\overline{T}(q(t)-q(t+\tau))\right]^2} \quad (6)$$

in which the subscript 'cor' indicates the corrected value and 'son' the sonic measurements. The specific humidity fluctuations are derived from open-path gas analyzers (LiCor-7500) placed at the same height as the sonics.

A disadvantage of using sonics to determine the structure parameter is that the temperature fluctuations smaller than the path length are not taken into account. To correct for these spectral losses, the correction of Hartogensis et al. (2002) for the deviation of the measured spectrum from the inertial subrange is used.

3.2.2 Turbulent Heat Fluxes

The turbulent fluxes are obtained from the sonic data, and in order to correct the turbulent heat flux for humidity, we use the first part of Eq. 12 of Liu et al. (2001). A tilt correction is applied as well. Streamline tilt is estimated by a linear regression between the mean vertical wind on the mean horizontal wind for wind-direction bins of 20° and for wind speeds $>3\,\mathrm{m\,s^{-1}}$. Fluxes are corrected given this wind-direction dependent mean streamline tilt. The turbulent fluxes are corrected for low frequency loss due to a finite averaging period. The correction is based on calculation of low-frequency contributions from standard surface layer cospectra (Bosveld 1999), extended to levels above the ASL by Schalkwijk et al. (2010).

3.3 The Scintillometer

An eXtra Large Aperture Scintillometer (XLAS Kipp & Zonen) has been set-up between the Cabauw Tower and the TV tower of IJsselstein (52°00.72′ N 5°03.23′E). The XLAS transmits a light beam with a near infra-red wavelength of 880 nm. The aperture diameter is 0.328 m. The distance between the two towers is 9.8 km. The terrain around Cabauw is flat and the height of the optical path above the surface is 59.9 m, which is the average of the receiver (61.7 m) and transmitter height (62.1 m) minus 2 m, which accounts for the earth's curvature along the path (Kohsiek et al. 2002).

To calculate the structure parameter of temperature from the structure parameter of the refractive index of air (C_{n^2}) (the primary output of the scintillometer), the following approximation can be used (Wesely 1976; Moene 2003):

$$C_{T^2}=C_{n^2}\frac{T^2}{A_T^2}\left(1+\frac{0.03}{\beta}\right)^{-2} \quad (7)$$

in which β is the Bowen ratio and $A_T\approx -0.78\ 10^{-6}p/T$ where p is the surface pressure. The Bowen ratio is determined from the turbulent fluxes at 60 m observed with the sonic and the LiCor. For the temperature we use the 10-m temperature. The Bowen-ratio correction ($(1+0.03/\beta)^{-2}$), which is a correction for humidity-related scintillations) is not applied for $\beta\approx -0.03$ ($-0.04<\beta<-0.02$), since C_{T^2} becomes numerically unstable when β approaches -0.03.

4 Results

4.1 The Structure of the Boundary Layer

In order to understand the relationship between surface fluxes, local-level fluxes and the observed temperature structure parameters, we first need to study the dynamics of the boundary layer and the different fluxes separately. In this section first the depth of the boundary layer is discussed. Next, the temporal evolution of the friction velocity, an important variable in MOST, is studied. Finally, the turbulent heat fluxes and the measured C_{T^2} at the four different levels are investigated.

The development of the boundary layer is quite similar for the eight days studied. The boundary layer starts growing around sunrise (0600 UTC) with its depth reaching 600 m between 0930 UTC and 1030 UTC. Thus only in the early morning is the 60-m level not located in the surface layer. Then, the boundary layer grows rapidly: between 1000 UTC and 1100 UTC the boundary layer reaches 1,000 m in depth. A few hours before sunset, the boundary-layer depth reaches its maximum around 2,000 m.

The composite diurnal cycle of the friction velocity is plotted in Fig. 3. During the night, the friction velocity is relatively small between 0.1 and 0.2 $\mathrm{m\,s^{-1}}$, whereas during the day higher values are observed. It is remarkable that $u_{*\mathrm{ll},60\mathrm{m}}$ is almost twice that of $u_{*3\mathrm{m}}$, around 0.55 and 0.3 $\mathrm{m\,s^{-1}}$, respectively. This is caused by the difference between the near-tower roughness and the regional roughness (see Sect. 3.1). In the early morning a flux divergence in turbulent stress is observed between 60, 100 and 180 m. This is a result of a deceleration of the flow when the rising convective boundary layer entrains air from the free troposphere that has been accelerated during the night when air aloft was decoupled from surface friction.

Figure 4a presents the time evolution of the local-level turbulent heat fluxes at the four levels averaged over the eight days. As can be seen, the fluxes decrease with height in the morning period until 1100 UTC. The fluxes at the elevated levels deviate more than 10 %

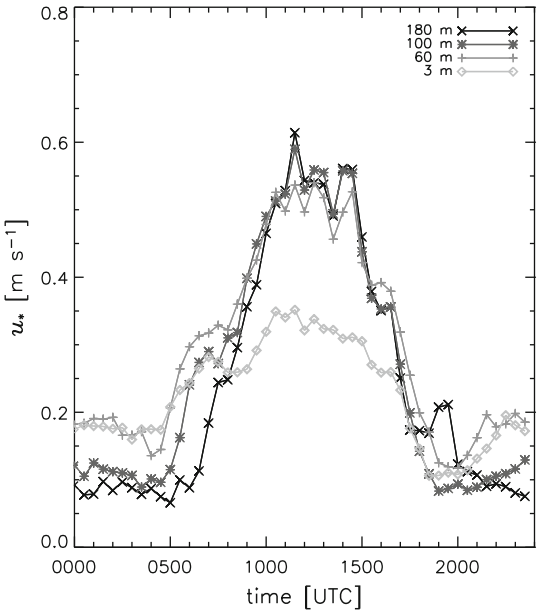

Fig. 3 The temporal evolution averaged over the eight days of the friction velocity ($u_{*\mathrm{ll}}$) at 3 m (*open diamond*), 60 m (*plus*), 100 m (*asterisk*) and 180 m (*cross*)

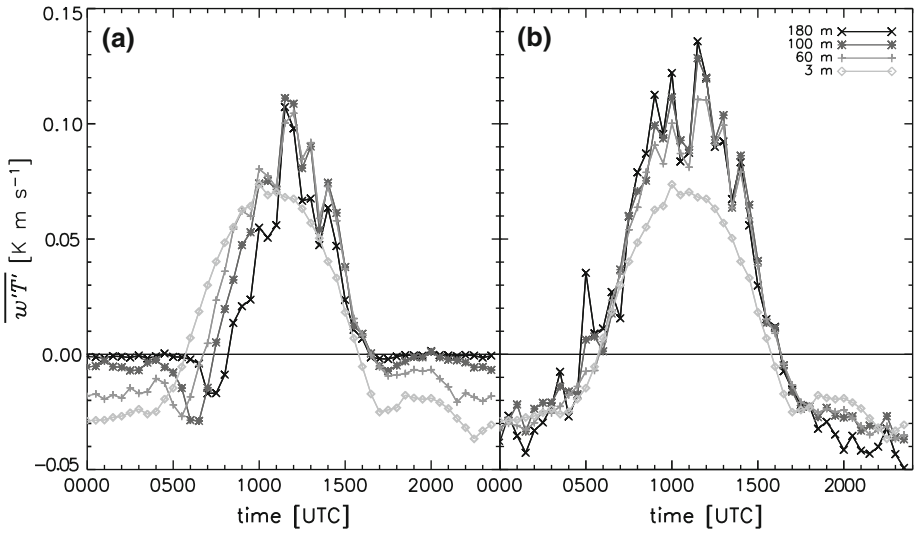

Fig. 4 The temporal evolution averaged over the 8 days of **a** the local-level turbulent heat flux ($\overline{w'T'}_{\mathrm{ll}}$) at 3 m (*open diamond*), 60 m (*plus*), 100 m (*asterisk*) and 180 m (*cross*) and **b** as in (**a**) but corrected for atmospheric storage below the sensor level ($\overline{w'T'}_{\mathrm{s}}$)

from the 3-m flux, as a result of the shallow surface layer and a large entrainment flux. For instance, at 0800 UTC the boundary-layer depth is almost 400 m, resulting in a surface-layer depth of 40 m. The entrainment flux could be estimated as almost $-0.06\,\mathrm{K\,m\,s^{-1}}$, by assuming a linear flux profile and using $\overline{w'T'}_{180\mathrm{m}} \approx 0$ and $\overline{w'T'}_{3\mathrm{m}} \approx 0.05\,\mathrm{K\,m\,s^{-1}}$. In other words, in the morning period the flux divergence is large and the application of MOST is questionable. On the other hand, after 1100 UTC the fluxes at different levels are more comparable. The values and the pattern of the 60- and 100-m fluxes are almost the same. The 180-m flux shows a comparable pattern. However, the values are almost 20 % lower from 1100 until 1500 UTC. From 1530 until 1700 UTC, when for most days the boundary layer was deeper than 1,800 m, the 180-m flux had the same values as the 60-m and 100-m fluxes.

The flux at 3 m is less variable than that at the other three levels. At 3 m the turbulent structures are much smaller than at the elevated levels. As a consequence more structures pass the sensor during the averaging time, resulting in statistically more stable values. Surprisingly, in the afternoon the 3-m flux is lower than the 60- and 100-m fluxes, and after 1400 UTC even lower than the 180-m flux. This deviation of the 3-m flux can also be observed in Fig. 4b. Figure 4b shows the 3-m flux together with the fluxes of the other levels, corrected for flux divergence. The corrected fluxes at 60, 100 and 180 m are quite comparable, especially in the afternoon from 1200 until 1800 UTC. The 3-m flux on the other hand is much lower during the entire day. A possible reason for the differences between the 3-m flux and that at the other levels might be that the instrument at 3 m measures a different footprint. Probably the soil of the surroundings is drier than the soil just around the tower, which leads to smaller latent heat flux and larger sensible heat flux at the elevated level when compared to 3 m. This is confirmed by further observations that show that the four levels give about the same total heat flux, where the 3-m level shows a different distribution of available energy over the latent and sensible heat fluxes (figure not shown). Thus, the near-tower terrain does evaporate more then the surrounding region. Hence, in Cabauw a distinction has to be made between the near-tower and regional Bowen ratios. In order to ensure comparable footprints between

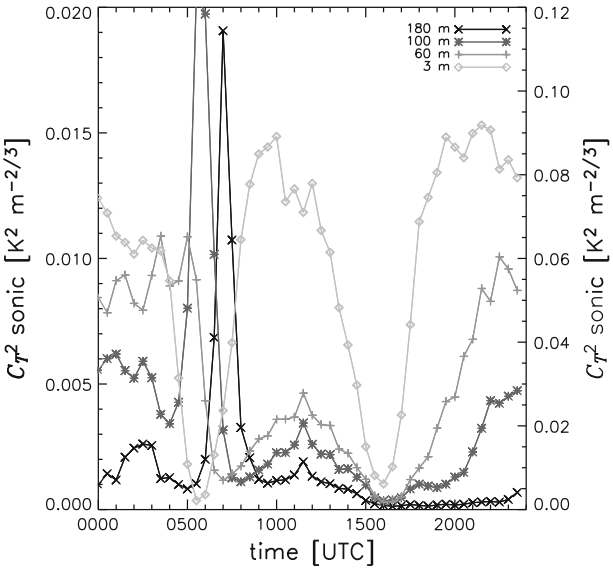

Fig. 5 The temporal evolution averaged over the 8 days of the direct measured structure parameter of temperature with sonics at 3 m (*open diamond*, right x-axis) and at 60 m (*plus*), 100 m (*asterisk*) and 180 m (*cross*) (all left-axis)

the surface flux and the local-level flux, in MOSTs the regional surface flux ($\overline{w'T'}_{\mathrm{s,60m}}$) is used.

Figure 5 shows the temporal evolution of the structure parameter of temperature at the four selected levels computed from the sonic data. C_{T^2} decreases with height, e.g. the values at 3 m are a factor of 10 larger than those at 60 m. The structure parameter of temperature has a clear diurnal cycle with a minimum observed in the morning and evening transition periods. In the morning sharp minima are observed around 0530 and 0700 UTC at the 3- and 60-m levels respectively, whereas at 100 and 180 m the minimum is less pronounced (0800 and 1000 UTC). In the evening the minima are found at 1600 UTC for the 3-m observations and at 1700 UTC at the other levels. Those minima are related to the minimum in temperature fluctuations under neutral conditions. Consequently the turbulent heat flux crosses zero at the same time (Fig. 4). At higher levels the minima in C_{T^2} correspond to the zero local-level turbulent heat flux and not to the surface flux at that moment, which by then already has a significant positive value (Fig. 4).

At 100 and 180 m the structure parameters have a large peak before they reach their minimum around 0600 and 0700 UTC, respectively. The observations at 60 m do not really show a peak, but still the C_{T^2} has a maximum at the end of the night (0500 UTC). Those maxima indicate strong temperature fluctuations, which occur at the moment that the particular level is located inside the entrainment zone. This is supported by the fact that the maxima at a specific level are observed at the moment when the turbulent heat flux at that level reaches its most negative value (Fig. 4a).

The early morning minima of C_{T^2} have larger values than the afternoon minima: around 1×10^{-3} and 2×10^{-4} K^2 m$^{-2/3}$ respectively. This is probably related to the nonstationarity of the morning transition. The large temperature variances that are created during the passage of the rising entrainment layer continue to influence C_{T^2}, even though the local stratification

is close to neutral. Thus during and just after the morning transition a direct relation between C_{T^2} and the sensible heat flux is not guaranteed.

These first results indicate that the structure parameter of temperature at a specific level shows a stronger relationship with the turbulent flux at that level than with the surface flux. This is in favour of the second concept: MOSTl.

4.2 The Proposed Similarity Relationships in the Surface Layer, Step 1

In this section we analyze the similarity relationships with (a) the 3-m data, and (b) the ASL data observed at 60 m from MOSTs and MOSTl (step 1, row 3, Fig. 2). Figure 6 shows the similarity relation between z/L and $C_{T^2} z^{2/3}/T_*^2$ for all unstable 30-min observations as well as the relationships proposed in the literature.

The 3-m data cover a stability range from $0.015 < -z/L < 0.46$. For 60 m we observe larger values for $-z/L$ ranging between 0.09 and 3. This is lower than a factor 20 (60/3), because apart from the difference in z we also use a different u_* and $\overline{w'T'}$ for the two measuring levels (see Sect. 3.1). During the day, $u_{*60\mathrm{m}}$ is around 1.6 to 1.8 times larger than $u_{*3\mathrm{m}}$ (see Fig. 3) and $\overline{w'T'}_{60\mathrm{m}}$ is a factor 1.5 larger than $\overline{w'T'}_{3\mathrm{m}}$ (see Fig. 4). All these differences imply that $-z/L$ is 6–9 times larger at 60 m than at 3 m.

Most scatter is found in the neutral region for both the 3-m data ($-z/L < 0.06$) and the 60-m data ($-z/L < 0.3$). For the 60-m data, even the relationship of H92 underestimates the measured values. Note that all the data points where $C_{T^2} z^{2/3}/T_*^2$ is > 8 are also located in the near-neutral range. The neutral data are observed during the morning and the late afternoon transition period when (a) the turbulent heat flux is small and measured temperature fluctuations are non-zero, and (b) the friction velocity is low. In other words, we do not observe neutral conditions because of a high wind speed, but because of a low sensible heat flux. The low heat flux means that the absolute error in the scaled structure parameter could be relatively large, which makes the neutral data more uncertain. Similar effects around near-neutral conditions for the relation between variances and fluxes were mentioned by Weaver (1990). On the other hand, our neutral data points are clustered above the similarity relationships from the literature, which is an indication that the error is a bias rather than a random error. Furthermore, DB93 found also a higher scatter and a slight overestimation during near-neutral conditions (see their Fig. 2). In order to further investigate the similarity relation under near-neutral conditions, observations are needed with a combination of large friction velocity and a larger sensible heat flux than those observed in our data.

Under unstable conditions ($-z/L > 0.06$), the 3-m data are centred around the similarity relationships of DB93 and A88, with H92 as the upper limit. The 60-m data are more centred around the similarity relationship of DB93. Moreover, a small difference between MOSTs and MOSTl is observed, since in spite of evaluating only ASL data the sensible heat flux at the two levels differ slightly (see Fig. 7a), with the values of MOSTl being marginally higher.

In order to investigate more systematically which of the proposed similarity relations we have to use with our dataset, the relationship $f\,(z/L) = c_1\,(1 - c_2 z/L)^{-2/3}$ is fitted to the data with an orthogonal distance regression method. Due to the limited range of z/L in our dataset, especially under neutral conditions, it is impossible to fit both coefficients simultaneously. We decide to fix c_1 because our dataset does not contain many near-neutral observations and those are also more uncertain than the unstable ones (see above). We tried two fits, the first with $c_1 = 8.1$ as proposed by H92 and the second with $c_1 = 4.9$ as in A88 and DB93.

Table 2 shows c_2 and their tolerance obtained from the two fits for the different ASL datasets. Furthermore, the relative deviation of our fitted coefficient ($c_{2\mathrm{fit}}$) from that obtained

Table 2 Values of the coefficient c_2 in the similarity relationships ($f\,(z/L) = c_1\,(1 - c_2 z/L)^{-2/3}$) obtained from a fit through the ASL data with an orthogonal distance regression method

Dataset	Fit 1: $c_1 = 8.1$				Fit 2: $c_1 = 4.9$				
				H92				A88	DB93
	$c_{2\mathrm{fit}}$	$c_{2\mathrm{Tol}}$	$\frac{c_{2\mathrm{Tol}}}{c_{2\mathrm{fit}}}$	$\frac{c_{2\mathrm{fit}}-15}{15}$	$c_{2\mathrm{fit}}$	$c_{2\mathrm{Tol}}$	$\frac{c_{2\mathrm{Tol}}}{c_{2\mathrm{fit}}}$	$\frac{c_{2\mathrm{fit}}-6.1}{6.1}$	$\frac{c_{2\mathrm{fit}}-9}{9}$
3 m	24.95	0.80	0.032	0.66	8.01	0.34	0.042	0.31	$\underline{-0.11}$
60 m MOSTs	20.12	0.89	0.045	0.34	8.64	0.44	0.051	0.42	$\underline{-0.04}$
60 m MOSTl	17.14	0.82	0.048	$\underline{0.14}$	7.26	0.42	0.058	0.19	−0.19

Fit 1 with a fixed c_1 of 8.1 as proposed by H92 ($c_{2\mathrm{H92}} = 15$) and fit 2 with a fixed c_1 of 4.9 as in the relationships from A88 ($c_{2\mathrm{A88}} = 6.1$) and DB93 ($c_{2\mathrm{DB93}} = 9$)
Underlined numbers indicate which literature value shows the lowest relative deviation for the given dataset

from the literature is given (columns 5, 9 and 10). We observe that $c_{2\mathrm{fit1}}$ varies from 17 to 25. The c_2 of our datasets is thus between 14 and 66 % larger than 15 observed by H92. The values of these deviations are quite high compared with the observed tolerance ranging between the 0.03 and 0.05. For $c_{2\mathrm{fit2}}$ we find a variation between 7.2 and 8.6.

In order to distinguish between fit 1 and fit 2, we calculate the relative difference in c_2 between the 3- and 60-m dataset ($(c_{2,3\mathrm{m}} - c_{2,60\mathrm{m}})/\overline{c_2}$). We make this comparison, because in the framework of MOST a variation of z/L through a variation in z should yield the same similarity relationship as when L is varied (as is normally done). We observe a larger difference for fit 1 than for fit 2 (using MOSTs for 60 m: 0.21 and −0.07, for fit 1 and fit 2 respectively, and using MOSTl: 0.37 and 0.10). Consequently, it seems that for our data $c_1 = 4.9$ is more consistent between the two levels than $c_1 = 8.1$. This can also be observed from Fig. 6: we observe a larger overestimation of the H92 relationship for the more neutral 3-m data than for the more unstable 60-m data. Further, the high values of $(c_{2\mathrm{fit}} - c_{2\mathrm{H92}})/c_{2\mathrm{H92}}$ compared with DB93 and A88 indicate that the relation of H92 is not the best similarity relationship to use for our dataset.

If we compare $(c_{2\mathrm{fit}} - c_{2\mathrm{A88}})/c_{2\mathrm{A88}}$ with $(c_{2\mathrm{fit}} - c_{2\mathrm{DB93}})/c_{2\mathrm{DB93}}$, we observe first that the fitted coefficient is larger than that of A88 and smaller than that of DB93. In other words, our fit is situated between A88 as an upper limit and DB93 as a lower limit. For the 60-m MOSTl dataset, $c_{2\mathrm{fit2}}$ is exactly located between the two proposed coefficients. Second, in general the overestimation of our fit compared with A88 is much larger than the underestimation compared with DB93. We conclude that our data best follows the relationship of DB93, and so we use this similarity relationship in the following section.

4.3 The Two Concepts Evaluated at 60 m, Step 2

Figure 7a presents a composite diurnal cycle of the 60-m regional surface heat flux ($\overline{w'T'}_{\mathrm{s},60\mathrm{m}}$) and the 60-m regional local-level heat flux ($\overline{w'T'}_{\mathrm{ll},60\mathrm{m}}$). Note that the heat flux is the only difference in the scaling between MOSTs and MOSTl (see row 2, Fig. 2). Figure 7b shows the composite diurnal cycle of the structure parameter of temperature measured directly from the sonic and the scintillometer and calculated with MOSTl and MOSTs using the similarity relationship of DB93.

Before evaluating the two concepts, we shortly compare the directly observed structure parameter of the scintillometer and the sonic, since the former is our motivation and the latter is used in our analysis. The two structure parameters show a quite comparable variation with time. Both instruments show a minimum at 0700 UTC of 1.2×10^{-3} K^2 m$^{-2/3}$ and at

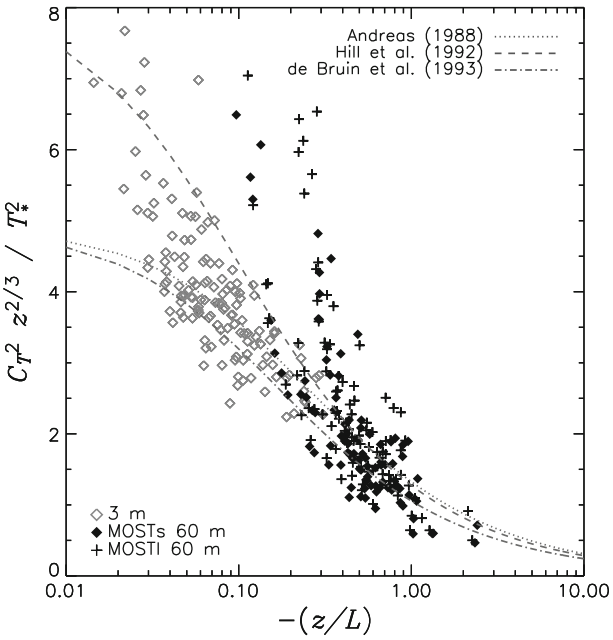

Fig. 6 The similarity relation obtained from the turbulent heat flux and the friction velocity at 3 m, (*open diamond*), at 60 m with MOSTs (*plus*), at 60 m with MOSTl (*filled diamond*), and three similarity relations proposed in the literature (*lines*). For the 3-m data, unstable conditions are selected: $\overline{w'T'}_{3\mathrm{m}} > 0$. For the 60-m data only data within the ASL are taken into account ($\overline{w'T'}_{60\mathrm{m}} > 0 \wedge z_{\mathrm{ASL}} > 60$). Data with $C_{T^2} z^{2/3}/T_*^2 > 8$ occur but are not shown for clarity (11 data points for 3 m and 6 data points for 60 m)

1600 UTC of 0.3×10^{-3} K^2 m$^{-2/3}$. When comparing the original 30-min data a coefficient of determination (r^2) is found of 0.71, which is quite large. The good comparison between the two instruments can be attributed to the relatively homogeneous surface around Cabauw. One difference is that the XLAS gives much smoother results, caused by the path averaging (Hartogensis et al. 2002). Furthermore, the XLAS shows slightly larger values than the sonic, which could be caused by surface inhomogeneity combined with different footprints for the two methods. But it could also suggest that the linear error (called high-C_{n^2}) found by van Kesteren and Hartogensis (2011) not only affects the Kipp & Zonen LAS but also the Kipp & Zonen XLAS. Nevertheless, to be consistent in our investigation we further only analyze the observations of the sonic, because the MOST-scaling variables are obtained from the sonic. Furthermore, the quite high level of agreement between the sonic and the scintillometer suggest that the conclusion of the coming analysis will be valid for the scintillometer data as well.

First, we investigate the concept MOSTs, since here MOST is applied in a standard way. By evaluating the ASL data (afternoon period) we observe (Fig. 7b) that the calculated structure parameter of temperature is comparable to the directly measured one. This observation is confirmed by the scatter plot of Fig. 8a. Figure 8a shows C_{T^2} determined with MOSTs against the one directly measured with the sonic. The coefficients of the best linear fit, the coefficient of determination (r^2) and the coefficient of variation of the RMSD (CV) are shown in Table 3. The coefficient of determination is a measure of the correlation, whereas CV indicates how much the data deviates from the 1:1-line. Notice that for Fig. 8 single data points are used instead of the composite of the 8 days. The linear fit for the ASL data is located near the

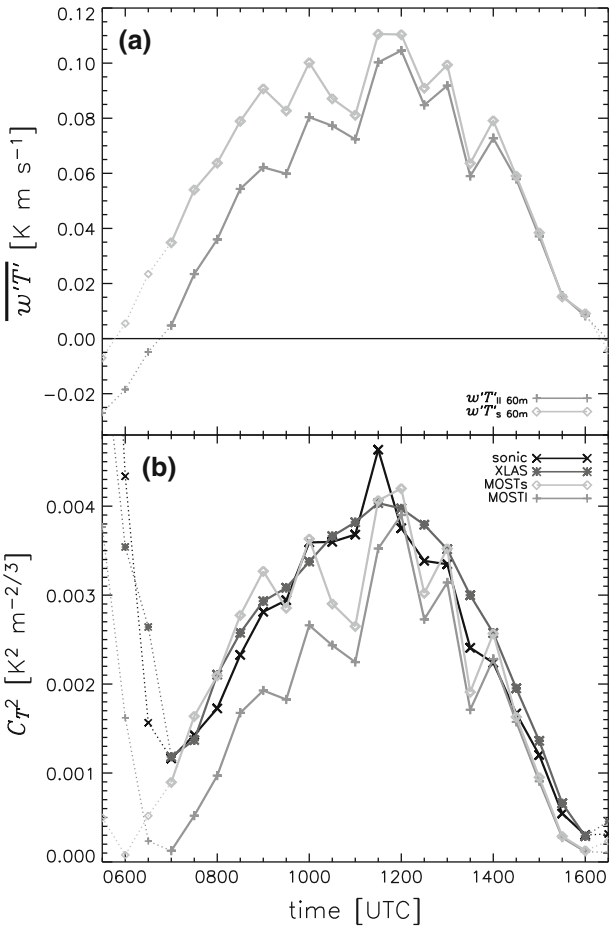

Fig. 7 The temporal evolution of **a** $\overline{w'T'}_{s,60m}$ (*open diamond*) and $\overline{w'T'}_{ll,60m}$ (*plus*) and **b** C_{T^2} measured with the sonic (*cross*) and the XLAS (*asterisk*) and calculated with MOSTs (*open diamond*) and MOSTl (*plus*) averaged over the eight days. In MOST the similarity relationship of DB93 is used, note that for $-z/L < 0$ (*thin lines*) the relationship for stable conditions is used

1:1-line, indicating that within the surface layer MOSTs gives reliable results. Furthermore, we observe that for small values ($C^2_{T\,\mathrm{sonic}} < 1 \times 10^{-3}$ K^2 m$^{-2/3}$) MOSTs underestimates the observed values. These data correspond to the neutral conditions during the evening transition (as a consequence of a low sensible heat flux instead of a high u_*).

Analyzing the NASL data (morning period) Fig. 7 shows that $C_{T^2\mathrm{MOSTs}}$ has a minimum at 0600 UTC when $\overline{w'T'}_{s,60m}$ approached zero (Fig. 7a). This is 1 h before the minimum in $C_{T^2\mathrm{sonic}}$. Moreover, from 0700 until 1000 UTC MOSTs overestimates the observations. From Fig. 8a we observe that the overestimation is almost 14 %. From 0600 to 0700 UTC MOSTs underestimates $C_{T^2\mathrm{sonic}}$. This underestimation is not visible in the scatter plot of Fig. 8a, since in that plot only unstable data are shown. Notice that it is therefore important to plot a diurnal cycle as well, rather than to show scatter plots only. The coefficient of determination is 40 % lower for NASL data than for ASL data. Furthermore, the coefficient of variation of the RMSD (CV) is higher for NASL data, indicating that for the ASL data the values of

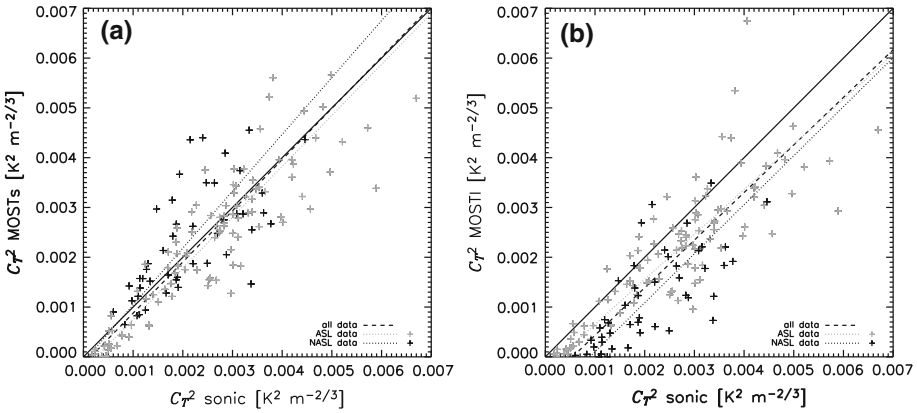

Fig. 8 The directly measured C_{T^2} from the sonic against the calculated C_{T^2} from MOSTs in (**a**) and MOSTl in (**b**) for observation inside (*grey*) and outside the surface layer (*black*). The *dashed line* represents the best fit through all the data, whereas the *dotted grey line* represents the best fit through the data inside the surface layer and the *dotted black line* outside the surface layer (see Table 3 for the functions). The *solid black line* is the 1:1-line

Table 3 The equations of the best linear fit through the 60-m data in Fig. 8 together with the coefficient of determination (r^2) and the coefficient of variation of the RMSD (CV)

	MOSTs			MOSTl		
All data	$y = 1.03x - 1.5 \times 10^{-4}$	$r^2 = \underline{0.70}$	CV = 0.32	$y = 0.96x - 5.2 \times 10^{-4}$	$r^2 = 0.69$	CV = 0.40
ASL data	$y = 1.02x - 2.7 \times 10^{-4}$	$r^2 = \underline{0.77}$	CV = 0.29	$y = 0.90x - 2.5 \times 10^{-4}$	$r^2 = 0.73$	CV = 0.35
NASL data	$y = 1.14x - 1.0 \times 10^{-4}$	$r^2 = 0.46$	CV = 0.40	$y = 0.98x - 8.8 \times 10^{-4}$	$r^2 = \underline{0.52}$	CV = 0.54

x is C_{T^2} from the sonic and y is C_{T^2} from MOST (similarity relationship of DB93)
Underlined numbers indicate which method shows the highest r^2 for the given dataset

MOSTs is closer to the observations than for NASL data. All in all, we can conclude that the surface sensible heat is not the correct scaling parameter for NASL data. Therefore, the second step is to evaluate MOSTl.

In this analysis we again make a distinction between the ASL data and NASL data. For the ASL data, we obtained from the composite diurnal cycle that $C_{T^2\mathrm{MOSTl}}$ is similar to $C_{T^2\mathrm{sonic}}$. The difference with MOSTs is relatively small. However, MOSTl shows slightly lower values because the local-level sensible heat flux is slightly lower than the regional surface sensible heat flux (see Fig. 7a). The small underestimation is also obtained from the scatter plot. The underestimation is around 10 % (the slope of the fit is 0.90). Consequently, the CV is also slightly higher than for MOSTs. In the end, we observe for MOSTl a relatively high r^2 of 0.73, similar to the value obtained for MOSTs.

Figure 7 shows that the $C_{T^2\mathrm{MOSTl}}$ has a minimum at 0700 UTC, as observed by $C_{T^2\mathrm{sonic}}$ as well. This is a first indication that the local-level sensible heat flux is a better scaling variable than the surface sensible heat flux in the transition morning period. Furthermore, the coefficient of determination and therefore the correlation is larger for MOSTl than MOSTs (0.52 and 0.46, respectively) for the NASL data during this morning period.

However, in spite of the comparable pattern during the morning transition, MOSTl underestimates the measured structure parameter by a factor of ten ($C_{T^2\mathrm{MOSTl}} = 1.26 \times 10^{-4}\,\mathrm{K^2\,m^{-2/3}}$ and $C_{T^2\mathrm{sonic}} = 1.16 \times 10^{-3}\,\mathrm{K^2\,m^{-2/3}}$ at 0700 UTC. This can also be

seen in the group of data points in Fig. 8b where $C_{T^2\text{sonic}}$ lies between 0.5×10^{-3} and 1.5×10^{-3} K^2 m$^{-2/3}$ whereas $C_{T^2\text{MOSTl}} \approx 0$. The structure parameter obtained with MOSTl shows a deep minimum due to the near-zero value of the local-level sensible heat flux. Therewith it misses the finite value of $C_{T^2\text{sonic}}$ that is probably due to ongoing transfer of temperature variance, previously produced within the entrainment zone (non-stationarity). Notice that MOSTs does not show the clustered data points in Fig. 8, but for the wrong reason. In Fig. 8 only unstable data are taken into account (see the solid lines in Fig. 7). Therefore the minimum of MOSTs, which is as low as the one for MOSTl, is not present in Fig. 8. During the rest of the morning period (0730–1100 UTC), MOSTl is in general 1×10^{-3} K^2 m$^{-2/3}$ lower than the observations (see the offset in the linear fit equation). The coefficient of variation of RMSD is also 36 % higher than for MOSTs (0.54 instead of 0.40). This suggest that MOSTs is on average closer to the observations than MOSTl, and the overestimation of MOSTs is smaller than that of MOSTl.

Overall, outside the surface layer neither of the two concepts provides a useful relationship between C_T^2 and the sensible heat flux.

5 Discussions and Conclusions

We investigate whether MOST can be used to obtain the surface sensible heat flux from elevated structure parameter data (in our case at 60 m). In this analysis two time periods are distinguished: the early morning and the afternoon. During the afternoon the 60-m level is located in the ASL (assumed to be the lowest 10 % of the boundary layer) and MOST is valid. During the morning the application of MOST is not always justified for two reasons. First, the observation height can be larger than 0.1 of the boundary-layer depth. Second, the divergence of the turbulent heat flux within the ASL can be considerably higher than in the afternoon due to relatively strong entrainment. Therefore, the strict definition of the surface-layer height ($z_{\text{ASL}} = 0.1 z_{\text{i}}$) does not imply that below that level the fluxes differ less than 10 % (constant-flux layer). For instance, in the free convection limit (entrainment ratio of -0.2) or during the morning, when entrainment is strong (e.g. entrainment ratio of -1.2) the fluxes differ 12 % or 22 %, respectively, within this layer. In other words, in our study the definition of the ASL is stretched and the fluxes could vary by more than 10 % in that layer.

Two theoretical concepts are proposed and compared. In the first concept (MOSTs), we assume that C_{T^2} at 60 m scales with the surface flux. In the second concept (MOSTl) C_{T^2} is scaled with the local-level sensible heat flux. Stability in the two concepts is also based on the surface and local-level sensible heat flux respectively. On the other hand, both concepts share the same friction velocity in the formulation of stability, in this case based on the stress measured at the 60-m level.

First, we analyzed 3-m and 60-m ASL data only, in order to investigate which of the MOST relationships proposed in the literature (DB93, H92 or A88) is suitable. We find an overestimation of our data with respect to the three relationships under low-heat-flux neutral conditions during the morning and evening transition. The data points are clustered indicating that the overestimation is a bias rather than a random error. However, since our dataset contain only low-heat-flux neutral data the scaling of C_{T^2} under near-neutral conditions could not fully be investigated. Therefore, we would recommend to further investigate the MOST relationships under high-wind-speed neutral conditions.

With an orthogonal distance regression method a MOST relationship of the form $f\,(z/L) = c_1\,(1 - c_2 z/L)^{-2/3}$ is fitted to the data. First, we fixed c_1 with a value 8.1 and 4.8 based on the relationships found in the literature. Then, the values for c_2 are compared with

the coefficients of DB93, H92 and A88. In general the deviation is the smallest for DB93, and so we use the DB93 similarity relationship.

Second, we compare the pattern of C_{T^2} obtained from sonic observations, at the four levels. In the early morning when the observation level is in or close to the entrainment zone, the sonic observations show a remarkable behaviour in C_{T^2}. First, when the elevated level is located in the entrainment zone, observations at 100 and 180 m show a peak in C_{T^2} before they reach their minimum. Second, the minimum in C_{T^2} occurs when the local-level flux crosses zero, whereas the surface flux is already positive. Finally, the evening transition shows deeper minima of C_{T^2} than in the morning. These three observations suggest that temperature variations in the entrainment layer influence the structure parameter during the morning transition, which indicates that the surface flux is not the sole parameter that determines C_{T^2} at higher levels.

Finally, the observed C_{T^2} from a sonic is compared with C_{T^2} calculated from the two concepts. Comparing the two concepts during the morning (NASL data), both methods show a low correlation with the observed C_{T^2}. We observe that the minimum C_{T^2} of MOSTs occurs indeed one hour before the observations, whereas that for MOSTl occurs at the same moment. However, the minimum value of MOSTl is much lower than the observations. In other words, the pattern of C_{T^2} obtained from MOSTl is closer to that of the observations than that of MOSTs, but the values of MOSTl are too low. This indicates that, during the transition zone, additional temperature fluctuations are present that do have no relation with the scaling theory. The values of $C_{T^2\mathrm{MOSTs}}$ are more similar to $C_{T^2\mathrm{sonic}}$; we found a slight overestimation. For ASL data both concepts agree with the observations.

As stated before, we use the relationship of DB93, because for ASL data the deviations of our fits are in general a minimum for DB93. However, for MOSTl the deviations of the fitted c_2 relative to the literature values are similar for the different similarity relations (see Table 2). Some of the above results may differ if another similarity relationship (instead of DB93) is used. If using the relationship of H92 or A88, the structure parameter obtained from MOST becomes larger. This will improve the results of MOSTl, since the underestimation becomes less. As a consequence, for H92 and A88 the coefficient of variation of the RMSD (CV) of MOSTl is smaller than MOSTs. Other observations such as (a) the time when the $C_{T^2\mathrm{minimum}}$ is observed, (b) the large underestimation of $C_{T^2\mathrm{minimum}}$ obtained by MOSTl compared to the observations, and (c) the values for the coefficients of determination all give similar results for the proposed similarity relationships (see also Table 4 in Appendix). In other words, the main conclusions do not significantly change when using these other relationships.

To conclude, neither MOSTs nor MOSTl is the final answer to the question of how to calculate the surface flux from the structure parameter at elevated levels. When the elevated level is located within the surface layer, MOSTs and MOSTl perform equally well. But in the morning hours neither works well: MOSTs does not have the correct temporal behaviour, whereas MOSTl does not provide the correct value (probably due to the strong nonstationarity).

Acknowledgments We thank Frank Beyrich (Deutscher Wetterdienst) and Bert Holtslag (Wageningen University) and the anonymous reviewers for reading the manuscript and providing valuable comments. Further, we thank Henk Klein Baltink (Royal Netherlands Meteorological Institute) for providing the data of the boundary-layer depth and Eddy Moors (Alterra) for the use of the 100-m turbulent data. This work has been supported financially in part by the German Research Foundation in the framework of the project: 'Turbulent Structure Parameters over Heterogeneous Terrain—Implications for the Interpretation of Scintillometer Data'. Further financial support was provided in the framework of the project 'Integrated observations and modelling of Greenhouse Gas budgets at the national level in the Netherlands', part of the program 'Climate changes Spatial Planning'.

Table 4 As Table 3 but than for A88, H92 and DB93

	MOSTs	MOSTl
A88		
All data	$y = 1.28x - 2.0 \times 10^{-4}\, r^2 = 0.69\,\mathrm{CV} = 0.44$	$y = 1.18x - 6.6 \times 10^{-4}\, r^2 = 0.69\,\mathrm{CV} = 0.37$
ASL data	$y = 1.27x - 3.6 \times 10^{-4}\, r^2 = 0.76\ \mathrm{CV} = 0.38$	$y = 1.12x - 3.4 \times 10^{-4}\, r^2 = 0.73\ \mathrm{CV} = 0.34$
NASL data	$y = 1.44x - 1.3 \times 10^{-4}\, r^2 = 0.46\ \mathrm{CV} = 0.61$	$y = 1.23x - 1.1 \times 10^{-3}\, r^2 = 0.52\ \mathrm{CV} = 0.48$
H92		
All data	$y = 1.26x - 1.7 \times 10^{-4}\, r^2 = 0.70\,\mathrm{CV} = 0.42$	$y = 1.18x - 6.3 \times 10^{-4}\, r^2 = 0.69\,\mathrm{CV} = 0.36$
ASL data	$y = 1.26x - 3.0 \times 10^{-4}\, r^2 = 0.77\,\mathrm{CV} = 0.37$	$y = 1.11x - 2.8 \times 10^{-4}\, r^2 = 0.74\,\mathrm{CV} = 0.32$
NASL data	$y = 1.38x - 1.2 \times 10^{-4}\, r^2 = 0.46\,\mathrm{CV} = 0.55$	$y = 1.19x - 1.1 \times 10^{-4}\, r^2 = 0.52\,\mathrm{CV} = 0.48$
DB93		
All data	$y = 1.03x - 1.5 \times 10^{-4}\, r^2 = 0.70\,\mathrm{CV} = 0.32$	$y = 0.96x - 5.2 \times 10^{-4}\, r^2 = 0.69\,\mathrm{CV} = 0.40$
ASL data	$y = 1.02x - 2.7 \times 10^{-4}\, r^2 = 0.77\,\mathrm{CV} = 0.29$	$y = 0.90x - 2.5 \times 10^{-4}\, r^2 = 0.73\,\mathrm{CV} = 0.35$
NASL data	$y = 1.14x - 1.0 \times 10^{-4}\, r^2 = 0.46\,\mathrm{CV} = 0.40$	$y = 0.98x - 8.8 \times 10^{-4}\, r^2 = 0.52\,\mathrm{CV} = 0.54$

Appendix. Statistics of C_{T^2} Obtained from the Two Concepts Compared to the Observations for A88, H92 and DB93

The results, and therefore the conclusions, from Sect. 4.3 could change by using another similarity relationship. Table 4 shows the same statistics as in Table 3 but now for the three proposed similarity relationships (A88, H92 and DB93). Notice that, for completeness, we include the information of DB93, which is a repetition from Table 3.

References

Andreas EL (1988) Estimating C_n^2 over snow and sea ice from meteorological data. J Opt Soc 5:481–495

Beyrich F, Görsdorf U (1995) Composing the diurnal cycle of mixing height from simultaneous sodar and windprofiler measurements. Boundary-Layer Meteorol 76:387–394

Beyrich F, Kouznetsov RD, Leps J, Ldi A, Meijninger WML, Weisensee U (2005) Structure parameters for temperature and humidity from simultaneous eddy-covariance and scintillometer measurements. Meteorol Z 14:641–649

Bosveld FC (1999) The KNMI Garderen experiment: micro-meteorological observations 1988–1989. Scientific report WR 99-03. KNMI

Braam M (2008) Determination of the surface sensible heat flux from the structure parameter of temperature at 60 m height during day-time. Technical report TR-303. KNMI

Businger JA, Wyngaard JC, Izumi Y, Bradley EF (1971) Flux-profile relationships in the atmospheric surface. J Atmos Sci 28:181–189

de Bruin HAR, Kohsiek W, van den Hurk BJJM (1993) A verification of some methods to determine the fluxes of momentum, sensible heat, and water vapour using standard deviation and structure parameter of scalar meteorological quantities. Boundary-Layer Meteorol 63:231–257

Foken T (2008) Micrometeorology. Springer, Heidelberg

Gill Instruments Ltd. (2002) Omindirection (R3) & Asymmetric (R3A) research ultrasonic anemometer, user manual. Gill Instruments Ltd, Hampshire

Hartogensis OK, DeBruin HAR, Van de Wiel BJH (2002) Displaced-beam small aperture scintillometer test. Part ii: cases-99 stable boundary-layer experiment. Boundary-Layer Meteorol 105:149–176
Hill RJ, Ochs GR, Wilson J (1992) Measuring surface-layer fluxes of heat and momentum using optical scintillation. Boundary-Layer Meteorol 58:391–408
Klein Baltink H, Holtslag AAM (1997) A comparison of boundary-layer heights inferred from wind profiler backscatter profiles with diagnostic calculations using regional model forecasts. In: Proceedings EURASAP Workshop, 1–3 Oct 1997, Ris/o, Denemarken, pp 51–54
Kohsiek W (1988) Observation of the structure parameters C2T, CTQ, and C2Q in the mixed layer over land. Appl Opt 27:2236–2240
Kohsiek W, Meijninger WML, Moene AF, Heusinkveld BG, Hartogensis OK, Hillen WCAM, DeBruin HAR (2002) An extra large aperture scintillometer for long range applications. Boundary-Layer Meteorol 105:119–127
Kohsiek W, Meijninger WML, DeBruin HAR, Beyrich F (2006) Saturation of the large aperture scintillometer. Boundary-Layer Meteorol 121:111–126
Lee X, Finigan J, Kyaw TPU (2004) Handbook of micrometeorology, a guide for surface flux measurements and analysis. Kluwer Academic Publishers, Dordrecht
Liu H, Peters G, Foken T (2001) New equations for the sonic temperature variance and buoyancy heat flux with an omnidirectional sonic anemometer. Boundary-Layer Meteorol 100:459–468
Lumley JL (1965) Interpretation of time spectra measured in high-intensity shear flows. Phys Fluids 9:1056–1062
Meijninger WML (2003) Surface fluxes over natural landscapes using scintillometry. Ph.D. thesis, Wageningen University, Wageningen
Meijninger WML, Hartogensis OK, Kohsiek W, Hoedjes JCB, Zuurbier RM, DeBruin HAR (2002) Determination of area-averaged sensible heat fluxes with a large aperture scinillometer over a heterogeneous surface—flevoland field experiment. Boundary-Layer Meteorol 105:37–62
Moene AF (2003) Effects of water vapour on the structure function parameter of the refractive index for near-infrared radiation. Boundary-Layer Meteorol 107: 635–653. doi:10.1023/A:1022807617073
Moene AF, Meijninger WML, Hartogensis OK, Kohsiek W, DeBruin HAR (2004) A review of the relation describing the signal of the large aperture scintillometer. Technical report. Meteorology and Air Quality Group, Wageningen University, Wageningen, the Netherlands
Nieuwstadt FTM (1984) The turbulent structure of the stable, nocturnal boundary layer. J Atmos Sci 41:2202–2216
Schalkwijk J, Bosveld F, Siebesma A (2010) Timescales and structures in vertical transport in the atmospheric boundary layer. Technical report WR-2010-02. KNMI
Schotanus P, Nieuwstadt FTM, DeBruin HAR (1983) Temperature measurements with a sonic anemometer and its application to heat and moisture fluxes. Boundary-Layer Meteorol 26:81–93
Stull RB (1988) An introduction to boundary layer meteorology. Kluwer Academic Publishers, Dordrecht
Tennekes H (1973) A model for the dynamics of the inversion above a convective boundary layer. J Atmos Sci 30:558–567
van Kesteren B, Hartogensis OK (2011) Analysis of the systematic errors found in the Kipp&Zonen large aperture scintillometer. Boundary-Layer Meteorol 138:493–509
van Ulden AP, Wieringa J (1995) Atmospheric boundary layer research at Cabauw. Boundary-Layer Meteorol 78:39–69
Weaver HL (1990) Temperature and humidity flux-variance relations determined by one-dimensional eddy correlation. Boundary-Layer Meteorol 53:77–91. doi:10.1007/BF00122464. http://dx.doi.org/10.1007/BF00122464
Wesely ML (1976) The combined effect of temperature and humidity fluctuations on refractive index. J Appl Meteorol 15:43–49
Wyngaard JC (1973) On surface-layer turbulence. In: Haugen DA (ed) Workshop on micrometeorology. American Meteorological Society, Boston, pp 101–149
Wyngaard JC, Clifford SF (1977) Taylor's hypothesis and high-frequency turbulence spectra. J Atmos Sci 34:922–928